Proceedings of HT2005
2005 ASME Summer Heat Transfer Conference
San Francisco, California, USA, July 17-22, 2005

HT2005-72399

EFFECTS OF MULTIPLE REFLECTIONS ON HOLE FORMATION DURING SHORT-PULSED LASER DRILLING

Michael F. Modest
Department of Mechanical and Nuclear Engineering
The Pennsylvania State University
University park, PA 16802
Email: mfmodest@psu.edu

ABSTRACT

Beam guiding effects during laser drilling due to multiple specular reflections inside the hole are analyzed for the case of very short laser pulses (ns range). Specular reflections are valid for materials that retain a smooth surface during laser evaporation (small optical roughness compared to the laser wavelength). The problem is assumed to be 2D axisymmetric (unpolarized laser), with the hole geometry defined by nodal values connected through a cubic spline. The net radiative flux onto a surface node is determined through ray tracing methods. The resulting absorbed laser flux is combined with a simple quasi-one-dimensional conduction model (to assess the minor conduction losses) and an Arrhenius evaporation rate model, to predict hole development as a function of time through iteration. To stabilize this highly nonlinear and thus unstable problem (in numerical analysis as well as in experiments) the laser beam is diffused a small amount from the specular direction (to also account for the limitation that no beam can be focused down to a point), and by periodic slight smoothing of the irradiation levels. Results show that drilling rates are increased dramatically due to beam trapping for highly reflective materials, resulting in a more pointed hole profile.

Nomenclature

c	specific heat
C_1, C_2	constants in Arrhenius relation
d	specular reflection cone diameter
E_p	total pulse energy
$\mathbf{F}$	irradiation flux vector
F_0	radiation flux density at center of beam at focal plane
Fo	Fourier number (pulse time-to-diffusion time ratio)
Δh_{re}	"heat of removal" (enthalpy of evaporation)
$\hat{\mathbf{i}}, \hat{\mathbf{j}}, \hat{\mathbf{k}}$	unit vector in x y and z directions
k	thermal conductivity
$\hat{\mathbf{n}}$	unit surface normal
n	distance along surface normal, measured from surface
m	complex index of refraction, $m = n - ik$
M^2	beam quality parameters
N_c	sensible heat-to-laser power parameter
Q_n	(dimensionless) absorbed irradiation flux at surface
r	dimensionless radial coordinate
$s(r,t)$	(dimensionless) groove depth
$\hat{\mathbf{s}}$	unit direction vector
Ste	Stefan number (ablation energy-to-sensible heat ratio)
t	(dimensionless) time
T	temperature
T_{re}	evaporation (or decomposition) temperature
V_n	(dimensionless) ablation velocity at surface
w, u_0	$1/e^2$ radius of laser beam (at focal plane)
x, y, z	(dimensionless) Cartesian coordinates
α_H	thermal diffusivity
α	local effective absorptance at laser wavelength and incidence direction
β_∞	far-field beam divergence
λ	wavelength of laser radiation
ρ	density of the medium, or radial distance from specular direction

θ dimensionless temperature
θ_{sp} opening angle of specular reflection cone
ϕ azimuthal angle ($x = r\cos\phi, y = r\sin\phi$)

Subscripts

n normal incidence
re evaluated at evaporation (or decomposition) temperature
0 at focal plane
∞ evaluated at ambient conditions, or located far away

1 Introduction

Lasers have a variety of applications in modern technology because of their ability to produce high-power beams. Applications include welding, drilling, cutting, machining, medical surgery, and others. Modeling of laser drilling, cutting, and scribing has been addressed by a number of investigators. Simple one-dimensional drilling models have been given by Dabby and Paek [1] and Wagner [2]. Other approximate laser drilling models have been developed by von Allmen [3], Petring et al. [4] and others. Multiple reflections during laser drilling have also been addressed by a number of researchers. Ramanathan and Modest [5] used an approximate conduction and ablation model to simulate laser drilling with diffuse reflections, noting that the nonlinear feedback between irradiation and surface recession causes great instabilities even for purely diffuse reflections. Probably for that reason all investigations to date dealing with multiple specular reflections during laser drilling have used fake geometries to eliminate such instabilities: Milewski and Sklar [6] used ray tracing to model a V-shaped welding joint, while Lee et al. [7] used a cone to model an axisymmetric keyhole; Ho et al. [8, 9] considered a paraboloid of revolution; Ki et al. [10] used a somewhat more general evolving fake shape, and, finally, Solana and Negro [11] also considered an evolving shape, but used a somewhat arbitrary surface recession model to avoid instabilities. Interestingly, specular reflections during scanning laser operation (welding, scribing) cause less instabilities, since they gradually move out of the laser interaction zone, rather than building up under the laser. Bang and Modest [12–14] studied scribing of ceramics with specular reflections (with and without polarization effects), and Ki et al. [15, 16] modeled a 3D-keyhole for welding applications. Both Ramanathan and Modest [5] and Ki et al. [15, 16] noticed that, once the hole attains sufficient depth, the absorbed reflected irradiation density can exceed the absorbed direct irradiation by a factor of 10 or more, concentrating near the center of the beam. Apparently, this is independent of surface quality, since the first of these studies considered diffuse reflections, and the second one specular reflections. It is the purpose of the present work to study the effects of multiple, quasi-specular reflections on the drilling of deep, high aspect ratio holes with a short pulsed laser (ns range). Realizing that no real surface is a truly specular reflector, a "quasi-specular" reflector reflects its energy into a small cone centered around the specular direction, with Gaussian decay away from it. This results in a somewhat smoothened distribution of reflected energy and, therefore, helps keeping the predicted drilling front stable. Nevertheless, some very minor additional smoothing of the irradiation profile is required to retain stability. This is to be expected: experimental evidence suggests that the slightest inhomogeneity (in material or beam stability) can lead to vastly different (and strangely shaped) holes. As such, the discussion here should be understood as qualitative, showing the most likely hole shape in a reasonably homogeneous material irradiated by a stable laser beam.

2 Theoretical Background

In order to obtain a realistic yet feasible mathematical description of the evaporation front that forms a high aspect ratio hole in a solid irradiated by a short-pulsed concentrated laser beam, several assumptions will be made:

1. The solid is isotropic with constant properties (evaluated at evaporation temperature). Since conduction losses are small during short pulse irradiation (ns range), this assumption should be a good one.
2. The material is opaque, i.e., the laser beam does not penetrate appreciably into the medium. This assumption is good for metals; for other materials, such as ceramics, slight penetration (of a μm or so) could easily be incorporated into the conduction model, but is not expected to have a noticeable effect on the results [17].
3. The change of phase from solid to vapor occurs in a single step governed by an Arrhenius reaction rate. During ns pulse irradiation the thickness of the heat affected zone is of the order of 1μm; thus, if a liquid layer exists it must be entirely too thin to modify the results [17].
4. The evaporated material escapes from the hole and does not interfere with the incoming laser beam, i.e., the optical thickness of the plume is very small at the laser wavelength and during laser on-time. Assuming all material to escape is perhaps the weakest assumption: while plasma formation may be limited for ns pulses, it is quite possible that some of the evaporated material cannot escape from the large aspect ratio hole, but recondenses higher up at the hole wall.
5. Heat losses by convection and reradiation are negligible (as compared to change-of-phase and conduction losses). This has been shown to be accurate even for CW laser operation [18].
6. At the surface, the laser beam is reflected in a quasi-specular fashion, i.e., reflection is within a small cone centered around the specular direction, with clipped-Gaussian intensity away from the specular direction. This serves two purposes: (i) no real surface can be expected to be optically smooth, and (ii) specular reflection from an axisymmetric hole wall would lead to the focussing of an irradiation ring

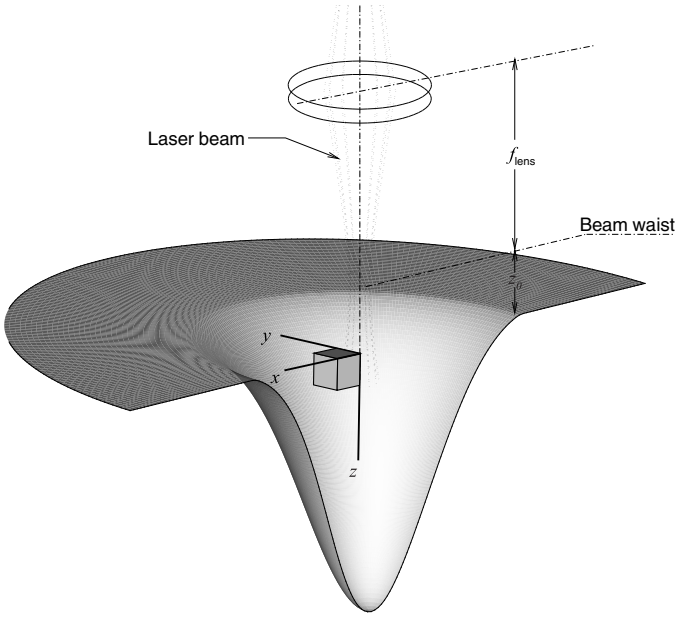

Figure 1. Laser drilling setup and coordinate system.

down to a single point, which is not possible and would lead to infinite absorbed intensity at the hole center. Surface reflectance is evaluated from Fresnel's relations, based on the material's complex index of refraction, m [19].

7. The laser beam is unpolarized, resulting in an axisymmetric (rather than three-dimensional) hole. In fact, most lasers are circularly polarized, which, at the first reflection, behave exactly like an unpolarized beam. However, after several reflections (as are bound to occur in deep holes) the beam becomes partially polarized, resulting in seriously noncircular hole cross-sections [20]. It was shown that trepanning (rotating work piece against laser during drilling) results in essentially perfectly round holes, which is assumed here.

The laser beam is assumed to have a spatially Gaussian power distribution with an effective radius $w(z)$, diverging away from the waist, given by Kogelnik and Li [21] as

$$w^2(z) = w_0^2 + \beta_\infty^2 (z_0 + z)^2; \quad \beta_\infty = M^2 \frac{\lambda}{\pi w_0}, \tag{1}$$

where w_0 is the $1/e^2-$ radius at the focal plane (the waist) through which 86.5% (or $1 - e^{-2}$) of the beam's energy passes, β_∞ is the far-field beam divergence angle, z_0 is the distance between the focal plane of the lens and the material surface ($z_0 > 0$ for focal point above surface, and $z_0 < 0$ for focal point below surface), M^2 is a beam-quality factor ($M^2 = 1$ for a Gaussian laser), and λ is the wavelength of the laser (cf. Fig. 1).

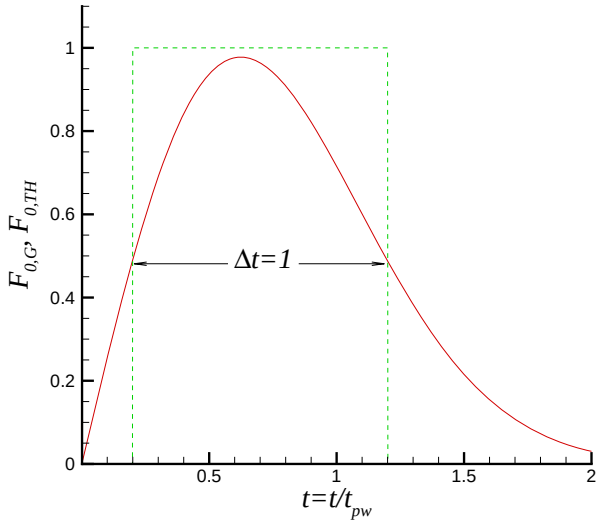

Figure 2. Temporal laser pulse shapes: top-hat and clipped-Gaussian profiles.

A Gaussian beam has a plane wave front at the waist (i.e., a radius of curvature of infinity) but assumes a curved wave front away from the beam waist. The radius of curvature of the wave front is:

$$r_c(z) = (z_0 + z)\left[1 + \frac{(w_0/\beta_\infty)^2}{(z_0 + z)^2}\right]. \tag{2}$$

If the laser beam is visualized as consisting of a bundle of rays, then the ray direction is normal to the wave front surface having curvature $r_c(z)$. The direct radiation from the laser may then be expressed as:

$$\mathbf{F}(x,y,z,t) = \left[\frac{w_0^2}{w^2(z)}\right] F_0(t) \mathrm{e}^{-2(x^2+y^2)/w^2(z)} \frac{\hat{\mathbf{s}}(x,y)}{\hat{\mathbf{s}} \cdot \hat{\mathbf{k}}} \tag{3}$$

$$\frac{\hat{\mathbf{s}}}{\hat{\mathbf{s}} \cdot \hat{\mathbf{k}}} = \frac{x\hat{\mathbf{i}} + y\hat{\mathbf{j}}}{\sqrt{r_c^2(z) - x^2 - y^2}} + \hat{\mathbf{k}} = \tan\gamma\cos\phi\hat{\mathbf{i}} + \tan\gamma\sin\phi\hat{\mathbf{j}} + \hat{\mathbf{k}},$$

where γ is the angle between a laser ray and the z-axis, ϕ is the azimuthal angle for the ray measured from the x-axis in the x–y plane, and $F_0(t)$ is the flux density at the beam center at the focal plane. Since, in the present simulation, an axisymmetric hole is considered, only beams lying in the x–z plane, or $\phi = 0$, need to be considered.

Two different temporal beam profiles are considered, viz., a simple top-hat profile and a clipped Gaussian profile (which

fairly accurately represents the temporal power distribution of a Q-switched Nd-YAG laser):

$$\text{Top-hat:}\quad F_0(t) = \begin{cases} F_{0\text{av}}, & 0 < t < t_{pw}, \\ 0 & t_{pw} < t < t_p, \end{cases} \tag{4a}$$

$$\text{Clipped Gaussian:}\quad F_0(t) = \begin{cases} F_{0\text{av}}\, a \frac{t}{t_{pw}} \mathrm{e}^{-b(t/t_{pw})^2}, & 0 < t < 2t_{pw}, \\ 0 & 2t_{pw} < t < t_p, \end{cases} \tag{4b}$$

where t_{pw} is the nominal pulse width (on-time with power levels larger than 50% of maximum, and t_p is the total pulse duration (i.e., on- and off-time); $F_{0\text{av}}$ is the average flux density at the beam center over the nominal pulse width, i.e.,

$$F_{0\text{av}} = \frac{1}{t_{pw}} \int_0^{t_p} F_0(t)\, dt; \tag{5}$$

for the clipped Gaussian profile the constants a and b are found from Eq. (5) and the condition that the pulse width at half of maximum is t_{pw}. Both profiles are compared in Fig. 2 (with the top-hat profile shifted for better comparison).

Following Modest [22, 23] the transient heat conduction equation for a thick solid irradiated by a laser beam, and its auxiliary conditions, may be written in nondimensional form as (slightly modified for the present drilling scenario using a short-pulsed laser):

$$\frac{\partial \theta}{\partial t} = \text{Fo} \nabla^2 \theta, \tag{6}$$

Initial condition:

$$t = 0 : \theta(r, z, 0) = 0 \qquad s(r, 0) = s_0(r), \tag{7}$$

Boundary conditions:

$$r, z \to +\infty : \ \theta = 0; \ z = s(r,t) : \ Q_n = N_c(V_n \text{Ste} - \text{Fo} \hat{\mathbf{n}} \cdot \nabla \theta); \tag{8}$$

Ablation condition:

$$z = s(r,t) : \ V_n = C_1 e^{C_2[1 - T_{\text{re}}/T(\theta)]}, \tag{9}$$

with

$$r = \bar{r}/u_0; \ z = \bar{z}/u_0; \ s = \bar{s}/u_0; \ t = \bar{t}/t_{pw};$$
$$\theta = \frac{T - T_\infty}{T_{\text{re}} - T_\infty}; \ Q_n = \frac{\bar{Q}_n}{F_{0\text{av}}} = \frac{\alpha \mathbf{F}_0 \cdot \hat{\mathbf{n}} + \bar{Q}_{\text{ref}}}{F_{0\text{av}}}; \ \text{Ste} = \frac{\Delta h_{\text{re}}}{c_p\,(T_{\text{re}} - T_\infty)}, \tag{10}$$
$$V_n = \frac{\bar{V}_n t_{pw}}{u_0}; \ \text{Fo} = \frac{\alpha_H t_{pw}}{w_o^2}; \ N_c = \frac{\rho c (T_{\text{re}} - T_\infty) u_0}{F_{0\text{av}} t_{pw}}.$$

Here $\bar{r}$, $\bar{z}$, and $\bar{s}$ are dimensional coordinates and groove depth (with the overbar shown only here in Eq. (10) to distinguish them from nondimensional ones), which are then nondimensionalized with the beam radius at the focal point, u_0; $\alpha_H = k/\rho c$ is the thermal diffusivity of the material, T_{re} is the equilibrium ablation (or "removal" temperature), and Δh_{re} is the energy required to remove material ("heat of removal", i.e., heat of vaporization in the simplest case). The parameter V_n is a nondimensional (transient) surface recession velocity (by ablation), Fo is the ratio between pulse duration and heat diffusion time, N_c approximates the ratio of sensible heating (due to conduction) and the incoming laser flux; and Ste is the Stefan number that compares ablation energy with sensible heat. The nondimensional absorbed radiation Q_n consists of two parts: a direct irradiation part (with α being the directional surface absorptance as calculated from Fresnel's relations [24]), and the contribution from multiple reflections, evaluated from ray tracing.

The boundary condition at the top surface, $z = s(r,t)$, specifies that absorbed laser irradiation is used up by conduction losses and by the latent heat required to ablate material. The ablation velocity (normal to the surface) is governed by a simple reaction equation of the Arrhenius type [22].

3 Solution Approach

Equation (6) with its auxiliary conditions (7)–(9) forms a complete set of dimensionless equations in transient form to predict the forming hole shape $s(r,t)$ and temperature field $\theta(r,z,t)$. In order to find a simple, approximate solution for the conduction loss, Eq. (1), we will assume that conduction takes place only in the direction of the (local) surface normal, i.e., the loss is locally one-dimensional. Transforming coordinates to n, a nondimensional distance from a surface location pointing into the medium along the local surface normal (see Fig. 3), the solid will move through the origin for n with the ablation velocity V_n into the negative n direction. Thus, Eq. (6) transforms to

$$\frac{\partial \theta}{\partial t} - V_n \frac{\partial \theta}{\partial n} = \frac{\partial^2 \theta}{\partial n^2}. \tag{11}$$

Equation (11) is solved iteratively together with Eqs. (8) and (9) by a simple finite difference scheme (using a tridiagonal solver). In order to do so the local heat affected zone thickness must be (conservatively) estimated: each pulse consists of a warmup period (without evaporation), during which time $n_{\max}$ is estimated as (conduction into a wall subject to constant flux)

$$n_{\max}(r,t) = 6\sqrt{\text{Fo}t}, \tag{12}$$

and an evaporation period, during which $n_{\max}$ remains essentially constant as (quasi-steady-state conduction with all energy going

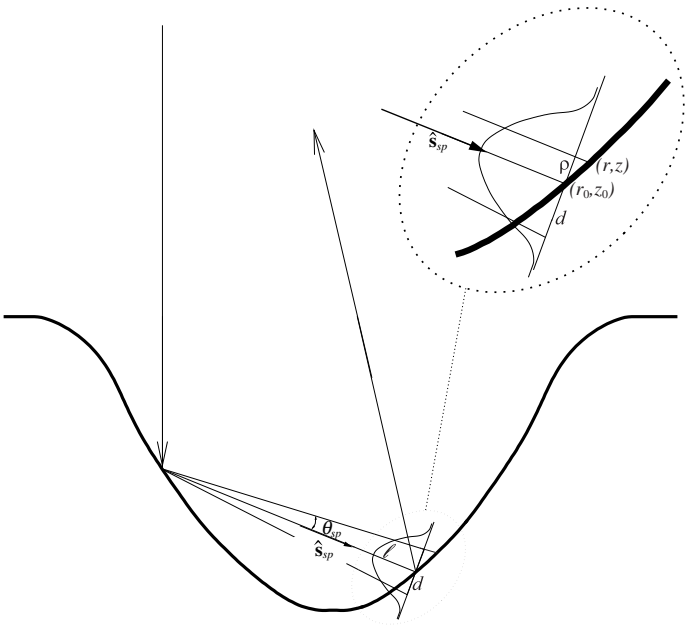

Figure 3. Specular reflection cone with Gaussian decay of strength away from specular direction.

into ablation)

$$n_{\max}(r,t) = 6\mathrm{Fo}(1+\mathrm{Ste})N_c/Q_n. \tag{13}$$

For this Eq. (11) is transformed one more time, using a new independent normal variable $\nu = n/n_{\max}$, leading to

$$\frac{\partial\theta}{\partial t} - \left(\frac{V_n}{n_{\max}} + \frac{\partial}{\partial t}\ln n_{\max}\right)\frac{\partial\theta}{\partial\nu} = \frac{1}{n_{\max}^2}\frac{\partial^2\theta}{\partial\nu^2} \tag{14}$$

$$z = s(r,t)\ [\nu = 0]: \frac{Q_n}{N_c} = V_n\mathrm{Ste} - \frac{\mathrm{Fo}}{n_{\max}}\frac{\partial\theta}{\partial\nu}. \tag{15}$$

For the finite difference solution values for θ and $n_{\max}$ must be stored for one time step.

Although the laser beam has a Gaussian intensity distribution and is best described by the wave equation [25], it may also be approximated as rays. The reflected direct irradiation is also assumed to consist of rays traveling along a straight path, i.e., the near-field phase information from wave theory is neglected. The total irradiation on the groove surface is then obtained by adding the direct irradiation calculated using Eq. (11) and the irradiation from multiple reflections. The reflected beam direction and the absorbed energy strongly depend on the surface normal and, therefore, on the method of surface representation. In the current study the hole is considered to be axisymmetric and, thus, only reflections in the x-z-plane are considered. The hole surface is described by two parametric cubic splines, each containing N_p (r,l)- and (z,l)-pairs, respectively, where l is arc length along the hole's surface. Such splines not only guarantee second-derivative continuity, but also allow multi-valued (r,z)-pairs. The latter is important for holes which have "throats," (i.e., the diameter below the surface is not monotonically decreasing, and there may be multiple z-values for a given r), as may occur due to focussing effects of multiple reflections. The spline knots (l positions) are updated periodically to keep them roughly equidistant (in arc length) even in very deep holes. This is always done between pulses, when the material is cold (and updating the internal temperature is not an issue). As indicated earlier, the interaction between irradiation and surface recession is extremely strong, with the slightest variation in hole shape causing great changes in reflected intensity and vice versa. Thus, to avoid statistical scatter, ray tracing with nonrandom emission positions has been used in the current study (rather than a standard Monte Carlo method). Several schemes were tried to simulate truly specular reflections, such as focussing/defocussing of an infinitesimal beam by a curved surface, collection of reflected rays by individual cells, etc. All these attempts resulted in unstable situations, as they should: for a deep hole there will always be a ray reflected off the side wall that hits the center of the bottom. In an axisymmetric hole this implies focussing a ring onto a point, resulting in infinite intensity and violating the laws of optics. It was, therefore, decided that the surface should not be treated as perfectly specular, but only preferentially specular, with Gaussian decay away from the specular direction $\hat{\mathbf{s}}_{sp}$. Consider a beam undergoing a first reflection, and then travelling on and hitting the hole wall again after a distance l, as shown in Fig. 3. If the beam carries a total energy of Q_b, then the beam energy density in a plane normal to $\hat{\mathbf{s}}_{sp}$ at location l is assumed to be

$$q_b \mathrm{e}^{-(\rho/d)^2}, \tag{16}$$

where ρ is radial distance away from the ray center in a plane normal to $\hat{\mathbf{s}}_{sp}$, and

$$Q_b = q_b \int_A e^{-(\rho/d)^2} 2\pi\rho d\rho = \pi d^2 q_b, \tag{17}$$

(where the second equality only holds if no beam shading occurs, which happens in deep grooves after several reflections and/or with too large cone opening angles). Thus, lines of equal intensity form circles in a plane normal to $\hat{\mathbf{s}}_{sp}$, an ellipse in a plane oblique to $\hat{\mathbf{s}}_{sp}$, and a somewhat more complicated

shape in a rotationally symmetric curved body (drill hole). This two-dimensional distribution of reflected energy needs to be accounted for. With some algebra and assuming, for a small cone angle θ_{sp}, that all beams in the cone hitting the hole wall travel parallel to $\hat{\mathbf{s}}_{sp} = s_x\hat{\mathbf{i}} + s_z\hat{\mathbf{k}}$, the cone radius ρ for a point on the wall $\mathbf{r} = r\cos\phi\hat{\mathbf{i}} + r\sin\phi\hat{\mathbf{j}} + z\hat{\mathbf{k}}$, with respect to a beam hitting point $\mathbf{r}_0 = r_0\hat{\mathbf{i}} + z_0\hat{\mathbf{k}}$ in the x-z -plane is determined from

$$\begin{aligned}\rho^2 &= |\mathbf{r} - \mathbf{r}_0 - ((\mathbf{r} - \mathbf{r}_0)\cdot\hat{\mathbf{s}})\,\hat{\mathbf{s}}|^2 \\ &= [(r\cos\phi - r_0)s_z - (z - z_0)s_x]^2 + r^2\sin^2\phi,\end{aligned} \tag{18}$$

and

$$Q_b = 2q_b \int_u \int_0^{\phi_{\max}} e^{-(\rho/d)^2}(\hat{\mathbf{s}}_{sp}\cdot\hat{\mathbf{n}})d\phi\, r\, du, \tag{19}$$

where $\hat{\mathbf{n}}$ is the outward surface normal at $\mathbf{r}$, and u is the arc-length along the hole wall in the x-z-plane. The value of the maximum azimuthal angle is $\phi_{\max} = \pi$, unless the beam hits the surface from behind ($\hat{\mathbf{s}}_{sp}\cdot\hat{\mathbf{n}} < 0$), in which case $\phi_{\max}$ is determined from

$$\hat{\mathbf{s}}_{sp}\cdot\hat{\mathbf{n}} = s_x n_x\cos\phi + s_z n_z = 0, \tag{20}$$

where $(n_x, 0, n_z)$ is the surface normal at (r, z) in the x-z-plane. The double integral in Eq. (18) is evaluated numerically for each (r, z)-cell by using a simple Newton-Cotes scheme in the u-direction (x-z-plane), and a 5-point Gaussian scheme ($\rho(\phi_{\max}) < 3.5d$) or a 5-point Hermitian scheme for the azimuthal integration. To conserve energy in the case of partial blockage, the q_b is adjusted so that all contributions add up to Q_b.

4 Results and Discussion

To investigate the effects of multiple specular reflections on drilling rates and hole geometry, a "typical" Nd-YAG laser, such as the Photonics Industries DS10-355 in our lab, with a Gaussian temporal pulse profile similar to the one shown in Fig. 1 with $t_{pw} = 4$ns was used which has an $M^2 = 1.88$ and, after focussing through a 50 mm lens onto the surface of the workpiece, has a beam radius of $w_0 = 13\mu$m. For most runs a pulse energy of $E_p = 100\mu$J was employed. As a representative material aluminum was chosen ($\alpha_H = 6.2\times10^{-5}$m^2/s, $\rho = 2700$ kg/m^3, $c = 1200$ J/kgK, $h_{\text{re}} = 13$ MJ/kg). This results in the following nondimensional parameters:

$$\beta_\infty = 0.036;\ \text{Ste} = 4.71,\ \text{Fo} = 1.5\times10^{-3},\ N_c = 0.250. \tag{21}$$

For the most part a refractive index of $m = 1.4 - 5.619i$ was used (with a normal absorptance of $\alpha_n = 0.15$) but, to test the influence of absorptance, values of $m = 1.4 - 7.088i$ ($\alpha_n = 0.10$) and $m = 1.4 - 4.716i$ ($\alpha_n = 0.20$) were also employed.

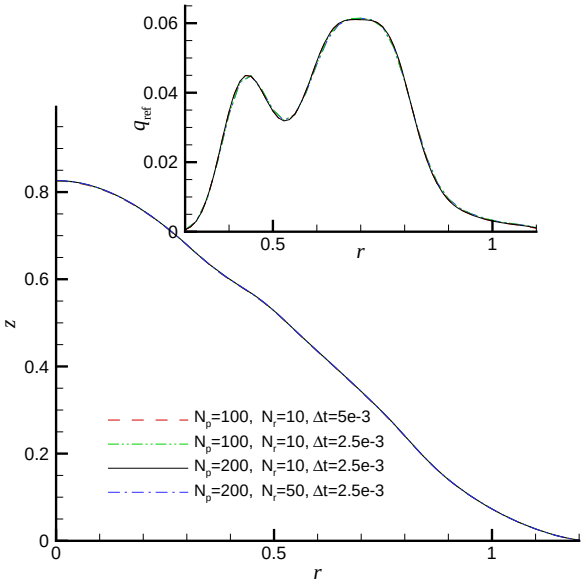

Figure 4. Influence of time step, cell number, and ray number on accuracy of solution during ns laser drilling.

Figure 4 shows the sensitivity of the solution to the number of radial nodes (N_p), number of rays traced per node (N_r) and the time step, all for 8 100μJ pulses, i.e., at a time when multiple reflections just start appearing, carving out a small bulge near $r = 0.5$ (here shown for a specular cone angle of $\theta_{sp} = 3°$). Also shown is the absorbed irradiation due to multiple reflections. It is seen that $N_p = 100$, $N_r = 10$ and $\Delta t = 5\times10^{-3}$ is more than adequate. However, it was observed that, for very deep holes, cumulative effects from a too large time step occurred, also causing worse instabilities. Thus, once the hole reached a certain depth, a much smaller time step of $\Delta t = 5\times10^{-4}$ was generally employed. In addition, $N_p = 200$ was used for deep holes to assure that nodes remained reasonably close together.

A similar sensitivity study is shown in Fig. 5, here studying the importance of conduction. It is seen that, whether 4 pulses at 200μJ or 8 pulses at 100μJ are used makes relatively little difference: the four-pulse holes are slightly deeper (less conduction loss), but the difference is small, since conduction losses are small. Similarly, the differences between tophat and Gaussian temporal profiles are small, with the Gaussian profile incurring larger conduction losses (since total pulse on-time is doubled). The differences are more pronounced in the reflected radiation profiles, indicating their sensitivity to the slightest variation in hole shape.

This sensitivity can be clearly observed in Fig. 6, which shows the absorbed specular reflections for one of the previous holes (8 pulses at 100μJ, top-hat laser profile) as a function of specular reflection angle θ_{sp}. For $\theta_{sp} = 3°$ two mild peaks are ob-

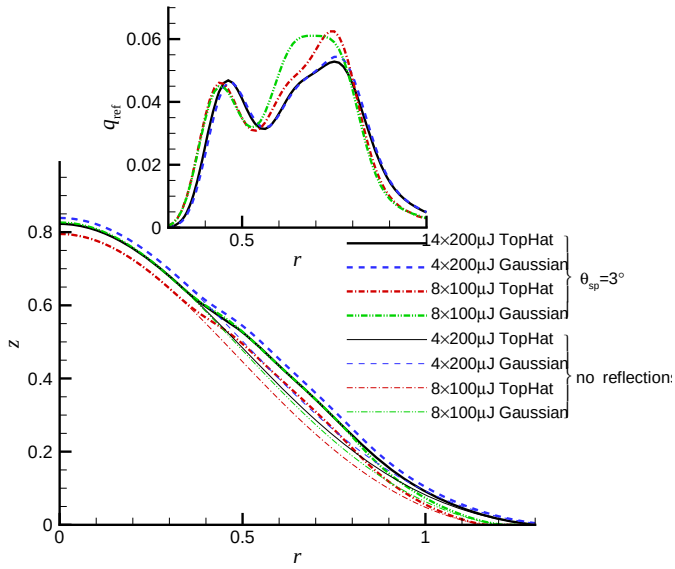

Figure 5. Influence of pulse strength and pulse temporal shape on conduction losses during ns laser drilling.

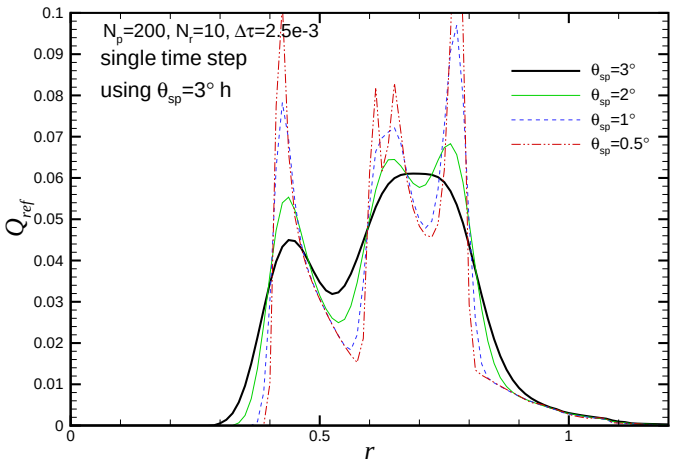

Figure 6. Influence of specularity angle on distribution of reflected energy inside laser-drilled hole.

served, but more and sharper peaks appear for smaller θ_{sp}. Such sharp irradiation peaks burrow small dimples into the hole walls, making the problem unstable within a few time steps. In Fig. 6 for all cases the same hole geometry was used (obtained by using $\theta_{sp} = 3°$ for drilling up to that point). If, say, $\theta_{sp} = 0.5°$ were taken from the beginning, the hole shape would still look essentially identical (little ablation due to reflected energy up to that point); but the reflected energy picture already resembles random

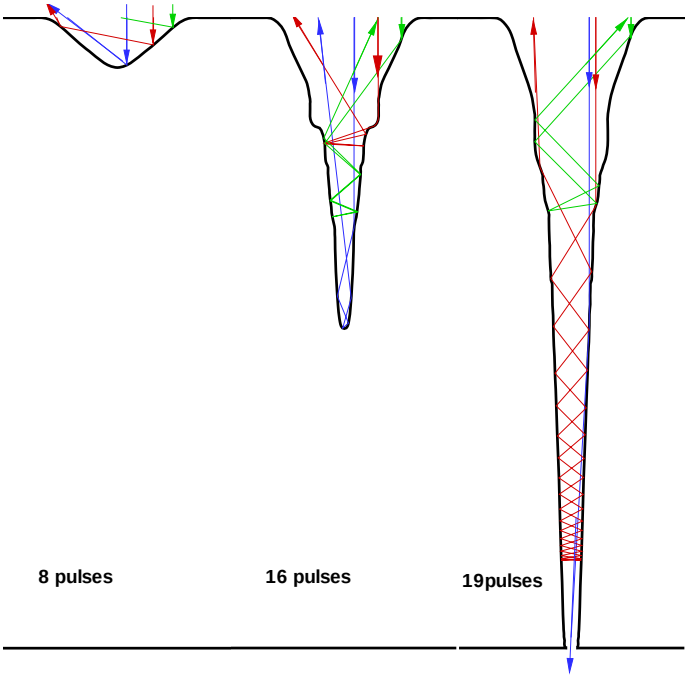

Figure 7. Typical laser ray reflection paths for varying hole depths (Ste = 4.71, $N_c = 0.25, \alpha_n = 0.15, \theta_{sp} = 5°$); a) hole after 8 pulses (without reflection effects), b) after 16 pulses (with bulging due to reflections), and c) after burn through (with strong beam trapping). Dimensions are to scale(with a material thickness of $10w_0$).

noise (not shown). Therefore, any deep drilling with a $\theta_{sp} \lesssim 5°$ should be expected to become unstable.

During drilling, as the hole gets deeper, multiple reflections first become important when the hole depth reaches about $s(0) \simeq 0.7$, with reflections hitting a ring with $r \gtrsim 0.5$ (with intensity decreasing toward $r = 1$ because of the grazing angles). This is shown in Fig. 7 for $\theta_{sp} = 5°$, and three typical ray paths are depicted in Fig. 7*a* for a shallow hole, showing that no beam undergoes more than one reflection. As the hole gets deeper multiple reflection intensity peaks occur, depending on specular angle θ_{sp}; for $\theta_{sp} \geq 5°$ generally only two peaks are present as long as the hole shape is relatively smooth; still no beam undergoes more than a single reflection. As the hole gets even deeper, the peak at the smaller r grows and slowly moves toward $r = 0$; now a number of beams start to have 2 and more internal reflections. Eventually, once the hole depth exceeds $s(0) \geq 1.5 - 2$, the reflection peak at the center becomes totally dominant, due to beams channeling near the center, as seen in Fig. 7*b*. Once the hole depth exceeds $s(0) \simeq 5$ the *average* number of reflections that a beam undergoes can be 10 or more. However, once the material is punched through, many beams escape through the bottom after only one or two reflections (Fig. 7*c*), and the reflection peak

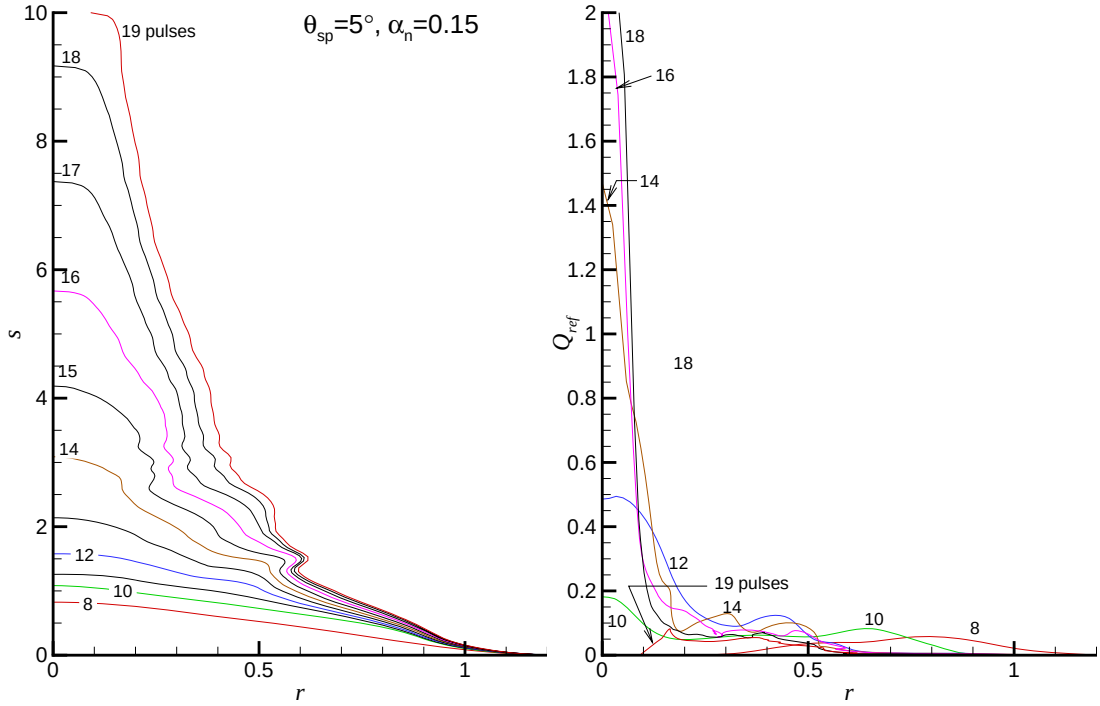

Figure 8. Hole development as a function of pulse number (Ste = 4.71, $N_c = 0.25, \alpha_n = 0.15, \theta_{sp} = 5°$); left: hole cross-section, right: absorbed, multiple-reflected laser power.

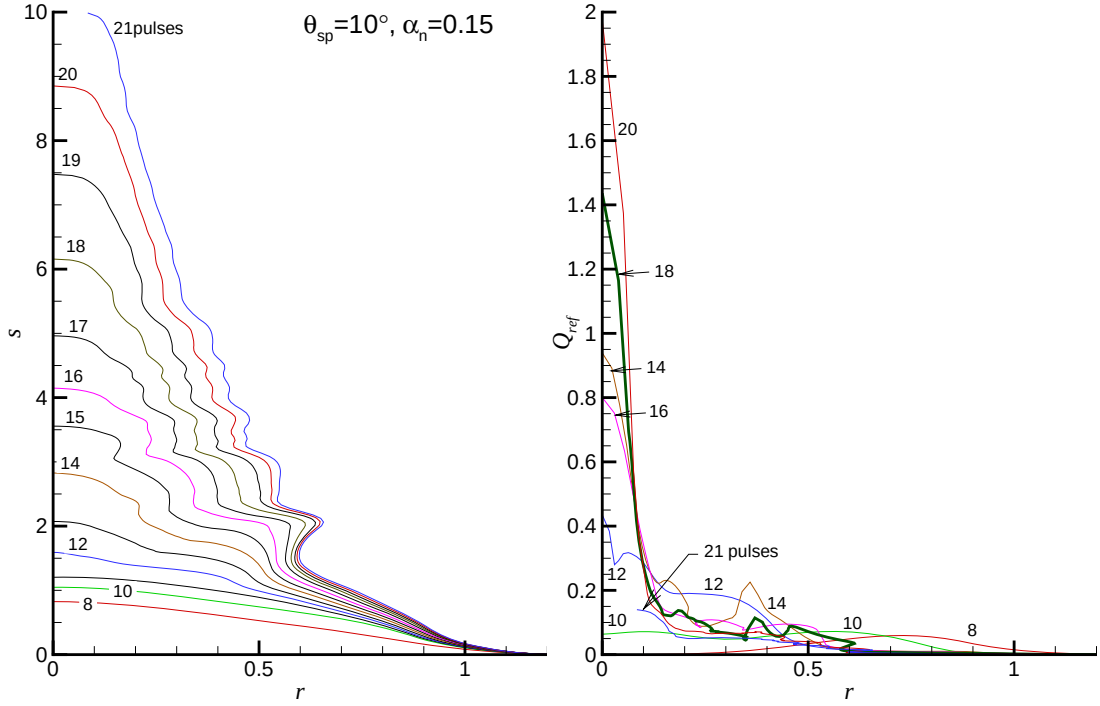

Figure 9. Hole development as a function of pulse number (Ste = 4.71, $N_c = 0.25, \alpha_n = 0.15, \theta_{sp} = 10°$); left: hole cross-section, right: absorbed, multiple-reflected laser power.

vanishes.

As a typical example of the drilling process, Fig. 8 shows the pulse-to-pulse progress of drilling through a $10w_0 = 130\mu$m thick aluminum film with a 100μJ laser, using a specular angle of $\theta_{sp} = 5°$, and an index of refraction of $m = 1.4 - 5.619i$ ($\alpha_n = 0.15$). Shown are hole cross-sections (left frame) and the locally absorbed amount of reflected radiation, both in nondimensional form and at the end of the (top-hat profile) pulse. As indicated earlier, multiple reflections do not occur until the seventh pulse (small single peak), and start becoming important after eight pulses (also depicted in Fig. 7*a*), showing two peaks (somewhat less pronounced than the $\theta_{sp} = 3°$ case shown in Fig. 5. As the hole deepens, a third peak appears and all peaks move toward the hole center until, after 12 pulses, the center peak dominates; however, a second, off-center peak remains for the duration of the drilling process, causing a bulge in the hole profile around $r \simeq 0.5$. Note how, after about 15 pulses beam channeling at the beam center becomes so strong to dramatically increase the drill rate per pulse. After 18 pulses a maximum Q_{ref} (= absorbed portion of multiple-reflected energy) of $2.6 \simeq 17\alpha_n$ is reached (i.e., 17 times the maximum possible direct irradiation), gradually decaying again for subsequent pulses. After burn-through, Q_{ref} drops dramatically, since a large portion of reflected beams escapes through the hole, Fig. 7*c*. In order to keep the calculations stable Q_{ref} was smoothened with a least-square-error spline whenever it displayed more than three off-center maxima. However, the smoothing range was limited to small changes, i.e., the smoothing would break down in the presence of 4 or more *large* off-center peaks. Under this scenario slight surface roughness still can occur and, for that reason, ablation velocity V_n was also smoothened (subject to the same conditions as Q_{ref}). This avoided smoothing of the hole shape itself (and thus avoiding possible negative ablation).

Figure 9 shows that changing the specular angle to $\theta_{sp} = 10°$ makes relatively little difference: the third peak after 10 pulses is washed out, and the general amplification near the beam center is somewhat lower. Therefore, 20 pulses rather than 19 are required for drill-through. Lowering the specular angle to $\theta_{sp} = 3°$, as shown in Fig. 10, also seems to yield little qualitative change, simply accentuating peaks and bringing down the drill time to 18 pulses. However, the off-center peaks tried to dig a secondary hole maximum near $r \simeq 0.1$, which required a little smoothening of the hole shape itself. Differences were also small due to the fact that no beam was allowed to focus to a spot smaller than $0.1w_0$, making many reflections in deep holes (with short distances between reflections) independent of small values for θ_{sp}.

Finally, Figs. 11 and 12 show the effects of raising or lowering the normal absorptance to 0.20 and 0.10, respectively. As expected, raising absorptance increases drill rates (16 pulse for drill-through), while lowering α_n decreases it (26 pulses). Qualitatively, the drilling behavior is the same for all three absorptances.

5 Summary and Conclusions

A two-dimensional, axisymmetric model was established to study the effects of multiple, specular reflections during evaporative drilling with ns laser pulses. To avoid the physically impossible focussing to a point, specularity was defined as reflection into a narrow cone with Gaussian decay away from the specular direction. Results show that, independent of specularity level, reflected energy levels exhibit a dual peak profile, with a peak at the beam center becoming more and more dominant as the hole gets deeper. Thus holes are formed which (i) exhibit a bulge away from the hole center, and (ii) totally absorb the laser's energy at the beam center due to many reflections, resulting in strong increases in drilling rates.

Acknowledgement

This work was supported by the Office of Naval Research, the Marine Corps contract number M67004-99-D-0037, Delivery Order 0089.

References

[1] Dabby, F. W., and Paek, U.-C., 1972. "High-intensity laser-induced vaporization and explosion of solid material". *IEEE Journal of Quantum Electronics,* **QE-8**, pp. 106–111.

[2] Wagner, R. E., 1974. "Laser drilling mechanics". *Journal of Applied Physics,* **45**, pp. 4631–4637.

[3] von Allmen, M., 1976. "Laser drilling velocity in metals". *Journal of Applied Physics,* **47**, pp. 5460–5463.

[4] Petring, D., Abels, P., and Beyer, E., 1988. "Absorption distribution on idealized cutting front geometries and its significance for laser beam cutting". In High Power CO_2 Laser Systems and Applications, SPIE, pp. 123–131.

[5] Ramanathan, S., and Modest, M. F., 1992. "CW laser drilling of composite ceramics". In Proceedings of ICALEO '91, Laser Materials Processing, Vol. 74, pp. 305–326.

[6] Milewski, J., and Sklar, E., 1996. "Modelling and validation of multiple reflections for enhanced laser welding". *Modelling Simul. Mater. Sci. Eng.,* **4**, pp. 305–322.

[7] Lee, J. Y., Ko, S. H., Farson, D. F., and Yoo, C. D., 2002. "Mechanism of keyhole formation and stability in stationary laser welding". *Journal of Physics D: Applied Physics,* **35**, pp. 1570–1576.

[8] Ho, C. Y., and Wei, P. S., 2001. "Absorption in a paraboloid of revolution-shaped welding or drilling cavity irradiated by a polarized laser beam". *Metallurgical and Materials Transactions,* **32B**, pp. 603–614.

[9] Ho, C. Y., 2004. "Effects of polarizations of a laser on absorption in a paraboloid of revolution-shaped welding or drilling cavity". *Journal of Applied Physics,* **96**(10), pp. 5393–5401.

[10] Ki, H., Mohanty, P. S., and Mazumder, J., 2002. "Multiple reflection and its influence on keyhole evolution". *Journal*

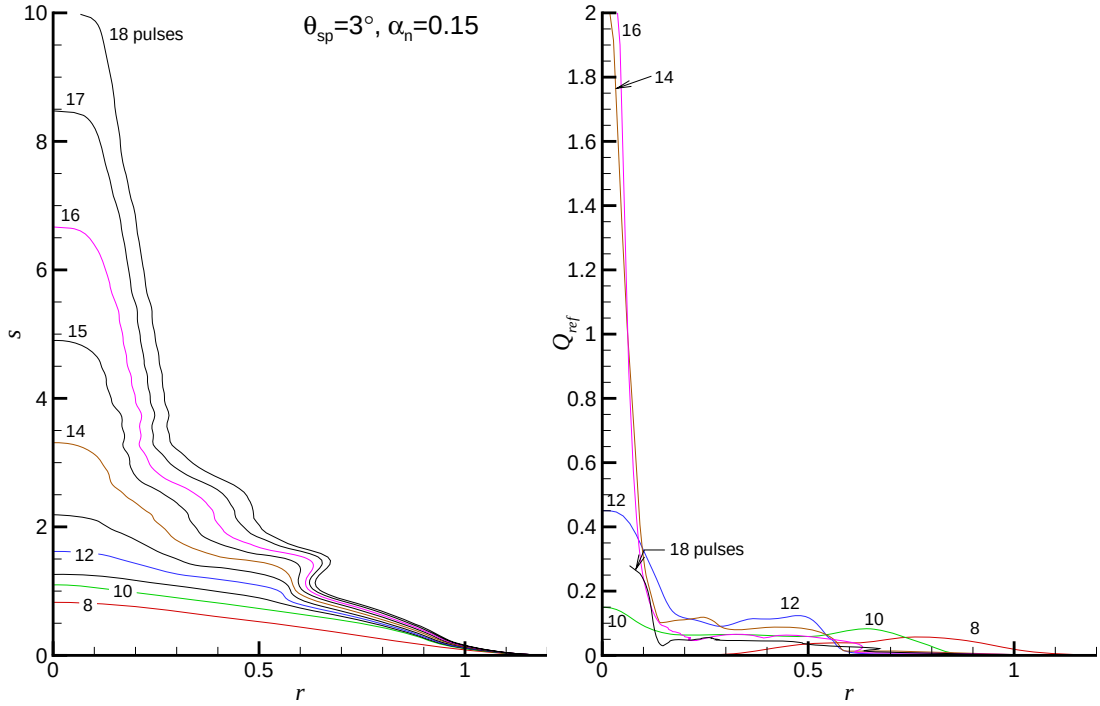

Figure 10. Hole development as a function of pulse number (Ste = 4.71, $N_c = 0.25, \alpha_n = 0.15, \theta_{sp} = 3°$); left: hole cross-section, right: absorbed, multiple-reflected laser power.

of Laser Applications, **14**(1), pp. 39–45.

[11] Solana, P., and Negro, G., 1997. "A study of the effect of multiple reflections on the shape of the keyhole in the laser professing of materials". *Journal of Physics D: Applied Physics,* **30**, pp. 3216–3222.

[12] Bang, S. Y., and Modest, M. F., 1992. "Evaporative scribing with a moving CW laser—effects of multiple reflections and beam polarization". In Proceedings of ICALEO '91, Laser Materials Processing, Vol. 74, pp. 288–304.

[13] Bang, S. Y., and Modest, M. F., 1991. "Multiple reflection effects on evaporative cutting with a moving CW laser". *ASME Journal of Heat Transfer,* **113**(3), pp. 663–669.

[14] Bang, S. Y., Roy, S., and Modest, M. F., 1993. "CW laser machining of hard ceramics — part ii: Effects of multiple reflections". *International Journal of Heat and Mass Transfer,* **36**(14), pp. 3529–3540.

[15] Ki, H., Mohanty, P. S., and Mazumder, J., 2002. "Modeling of laser keyhole welding: Part i. mathematical modeling, numerical methodology, role of recoil pressure, multiple reflections, and free surface evolution". *Metallurgical and Materials Transactions,* **33A**, pp. 1817–1830.

[16] Ki, H., Mohanty, P. S., and Mazumder, J., 2002. "Modeling of laser keyhole welding: Part ii. simulation of keyhole evolution, velocity, temperature profile, and experimental verification". *Metallurgical and Materials Transactions,* **33A**, pp. 1831–1842.

[17] Abakians, H., and Modest, M. F., 1988. "Evaporative cutting of a semi-transparent body with a moving CW laser". *ASME Journal of Heat Transfer,* **110**, pp. 924–930.

[18] Modest, M. F., and Abakians, H., 1986. "Evaporative cutting of a semi-infinite body with a moving CW laser". *ASME Journal of Heat Transfer,* **108**, pp. 602–607.

[19] Modest, M. F., 1993. *Radiative Heat Transfer*. McGraw-Hill, New York.

[20] Nolte, S., Momma, C., Kamlage, G., Ostendorf, A., Fallnich, C., Alvensleben, F., and Welling, H., 1999. "Polarization effects in ultrashort-pulse laser drilling". *Applied Physics A,* **68**, pp. 563–567.

[21] Kogelnik, H., and Li, T., 1966. "Laser beams and resonators". *Applied Optics,* **5**(10), pp. 1550–1567.

[22] Modest, M. F., 1996. "Three-dimensional, transient model for laser machining of ablating/decomposing materials". *International Journal of Heat and Mass Transfer,* **39**(2), pp. 221–234.

[23] Modest, M. F., 1996. "Transient model for CW and pulsed laser machining of ablating/decomposing materials—approximate analysis". *ASME Journal of Heat Transfer,* **118**(3), August, pp. 774–780.

[24] Modest, M. F., 2003. *Radiative Heat Transfer*, 2nd ed. Academic Press, New York.

[25] Verdeyen, J. T., 1981. *Laser Electronics*. Prentice Hall, Englewood Cliffs, NJ.

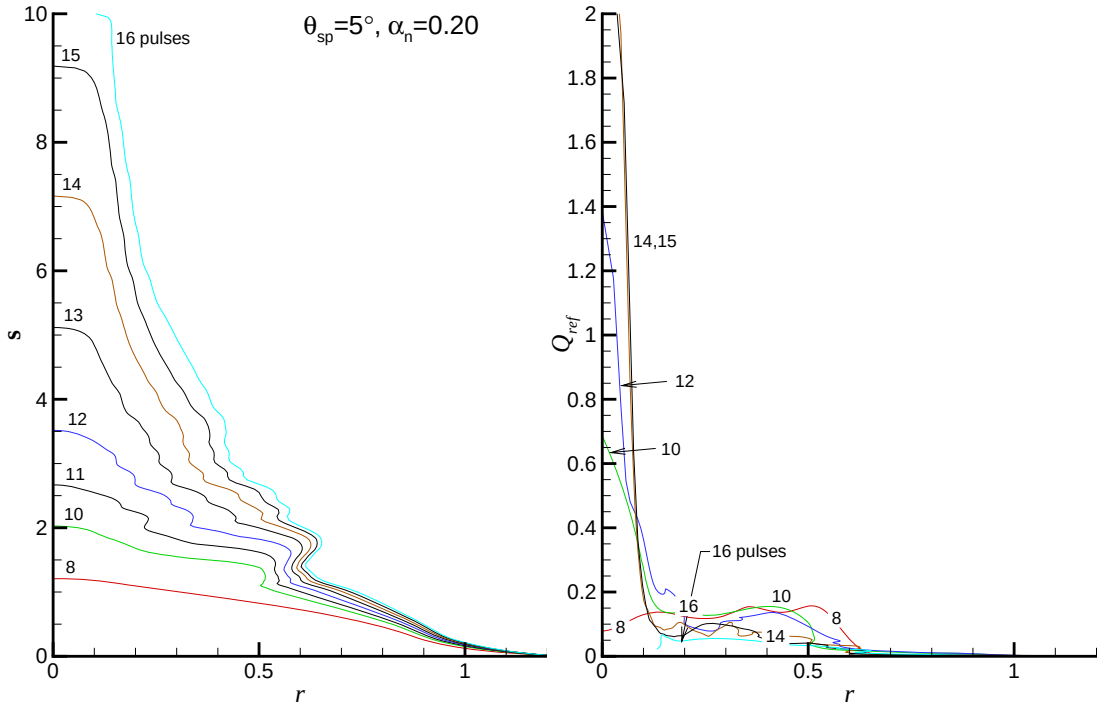

Figure 11. Hole development as a function of pulse number (Ste = 4.71, $N_c = 0.25, \alpha_n = 0.20, \theta_{sp} = 5°$); left: hole cross-section, right: absorbed, multiple-reflected laser power.

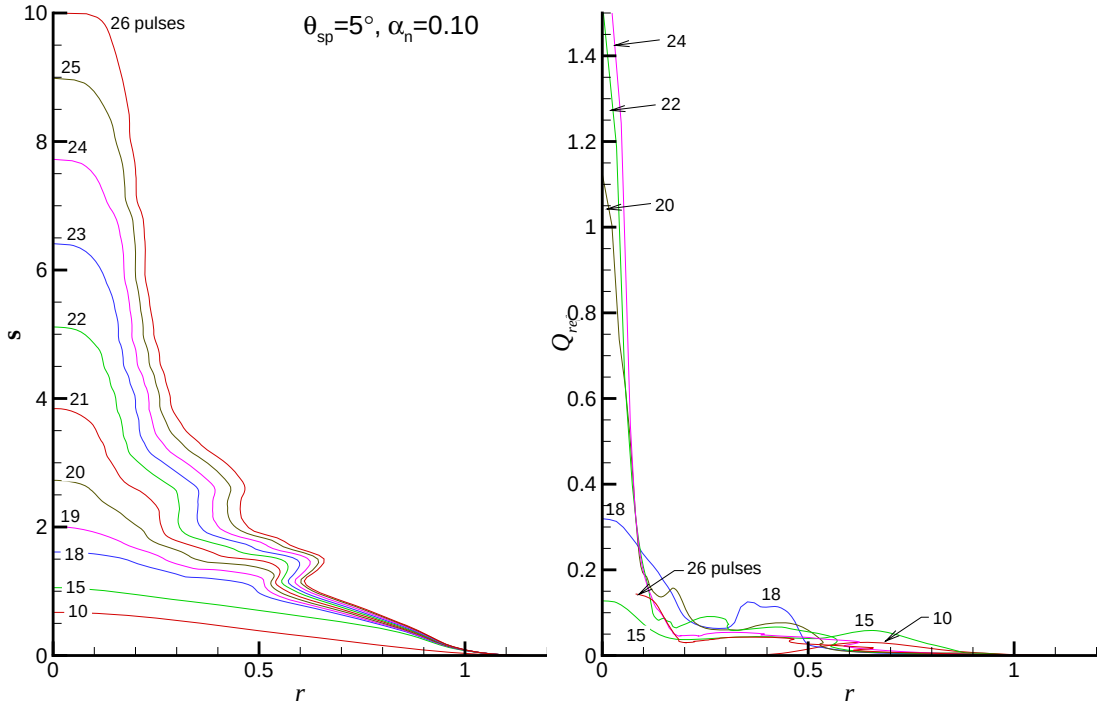

Figure 12. Hole development as a function of pulse number (Ste = 4.71, $N_c = 0.25, \alpha_n = 0.10, \theta_{sp} = 5°$); left: hole cross-section, right: absorbed, multiple-reflected laser power.